

# Quadrature Spatial Modulation Orthogonal Frequency Division Multiplexing

B.S. Adejumobi and N. Pillay

*School of Engineering, University of KwaZulu-Natal, Durban, South Africa, 4041  
adejumobi@ieee.org*

**Abstract**— This paper investigates the application of quadrature spatial modulation (QSM) to orthogonal frequency division multiplexing (OFDM). In comparison to spatial modulation OFDM (SM-OFDM), the proposed QSM-OFDM achieves an enhanced spectral efficiency by decomposing the amplitude and/or phase modulated signal into its real and imaginary components as the transmitted symbols. The index/indices of the activated transmit antenna(s) are employed to convey additional information. These symbols are transmitted orthogonally to eliminate inter-channel interference with little trade-off in synchronization. The average bit error probability for QSM-OFDM and other schemes, including the SM-OFDM, conventional multiple-input multiple-output (MIMO-OFDM), maximal-ratio combining single-input multiple-output (MRC-OFDM), vertical Bell Laboratories layered space-time architecture (VBLAST-OFDM) and Alamouti-OFDM systems are demonstrated using Monte Carlo simulation. The expressions for the receiver computational complexities in terms of the number of real operations are further derived. QSM-OFDM yields a significant signal-to-noise ratio gain of  $\approx 5$  dB with little trade-off in computational complexity over SM-OFDM, while substantial gains greater than 5 dB are evident, when compared to other systems.

**Index Terms**— Enhanced Multi-carrier Modulation; Maximum Likelihood Detection, Orthogonal Frequency Division Multiplexing; Quadrature Amplitude Modulation; Quadrature Spatial Modulation, Spatial Modulation.

## I. INTRODUCTION

Recent applications have placed a great demand for high data rates and spectral efficient systems with extremely low error rates; hence, there has been a rapid growth in research areas that deals with the improvement as well as technological advancement of future wireless systems. In many modern wireless communication systems, designers have resorted to employing high-order modulation schemes, such as  $M$ -ary quadrature amplitude modulation (MQAM). However, it becomes disadvantageous when high-order MQAM ( $M \geq 64$ ) is used. This is because of the destructive noise from the deployed equipment and channel fading [1]. The use of multiple-input multiple-output (MIMO) antenna arrangements, such as in WiMAX, HSPA, IEEE 802.11ac, etc., when combined with spatial multiplexing has become a very promising technique in achieving reliable and spectral efficient communications [2]. An example is Bell Laboratories layered space-time architecture (BLAST), where the transceiver architecture is designed, such that independent data is simultaneously transmitted employing different antennas, thereby leading to an increase in multiplexing gain [3].

MIMO can also be used to reduce error rates by simultaneously transmitting identical data from multiple

antennas as in space-time coding/space-frequency coding [4]. This is performed to exploit the advantage of having multiple received signals, which arrive at the receiver along different pathways. MIMO increases the transmit diversity and ensures reliability as well as sufficient quality-of-service. As noted in [5], MIMO systems such as BLAST, suffer from high inter-channel interference (ICI) because of the simultaneous transmissions from multiple antennas. Furthermore, due to high ICI, computational complexity in MIMO systems increases because of the need for complex receiver detection algorithms. The complexity cannot be reduced without a trade-off in the error performance of the system. To deal with the limitations offered by conventional MIMO as mentioned earlier, spatial modulation (SM) [5,6], generalized SM (GSM) [7], space shift keying (SSK) [8], generalized SSK (GSSK) [9] and generalized differential scheme for SM systems [10], were introduced as promising techniques to alleviate these limitations.

In SM, since only a single transmit antenna is activated at a given instant of time [5,10], this helps in eliminating ICI. The need for synchronization amongst the transmit antennas, as well as the complexity of detection at the receiver is reduced as SM utilizes a single radio frequency (RF) chain [11]. Comparing SM to other conventional MIMO techniques, it has been observed that SM techniques improve error rates even with limited transmit antennas and are robust in dealing with channel imperfections. SM systems [5,6,10] improve spectral efficiency by exploiting the index of the activated transmit antenna to convey additional information. Furthermore, employing a single antenna eliminates ICI as well as the need for synchronization at the transmitter. However, a major limitation of SM is that, the spectral efficiency does not increase linearly with the total number of transmitting antennas as in the case of vertical-BLAST (VBLAST). In GSM and GSSK [7,9], more than one antenna is allowed to transmit different symbols, using the antenna indices as a spatial constellation in the spatial domain but was found to be inferior to SM and SSK in terms of error performance. This is further improved in bi-space shift keying (Bi-SSK) modulation [12], such as to improve the throughput of the low-complexity receiver of the SSK system, with little trade-off in the error performance. In [13], the SM technique, which employs two time-slots, to transmit two symbols in each time-slot, has been considered; however, the complexity of the detection is significantly increased especially when the maximum-likelihood (ML) detector is applied.

In 2006, Ganesan et al. [14] proposed a scheme, where SM is combined with orthogonal frequency division multiplexing (OFDM). This is performed, to produce a spectrally enhanced, multicarrier system, which is robust to channel

imperfections [5,14] and yields an improved error performance [1]. The advantage of OFDM arises because the wireless channel is divided into several narrowband, low-rate, frequency non-selective subcarriers, which allows for the parallel simultaneous transmission of multiple symbols [15]. SM-OFDM utilizes the SM mapping style, where a group of information bits is mapped into an amplitude and/or phase modulation (APM) symbol and a transmit antenna, which is then transmitted using the MIMO-OFDM system [1]; such that, both the activated transmit antenna and the APM symbols are used to convey information [1,5,14]. The SM-OFDM scheme was tested for two different channel conditions; viz. Rician fading channel, and a combined effect of spatially correlated (SC) and mutually coupled (MC) channels. Furthermore, Mesleh et al. established the combined effect of all the three channels in [14]. Hwang et al. demonstrated the error performance of SM-OFDM using a soft-output ML detector [1]. In [16], precoders were utilized to improve error performance in SM-OFDM. Although SM-OFDM yields a significant improvement in error performance over existing schemes, there is still room for improvement.

A new technique of quadrature spatial modulation (QSM), proposed in [17] to improve the throughput of SM, was achieved by extending the spatial constellations of SM to the in-phase and quadrature components by utilizing methods as in [5,7,12]. One of the antennas is made to transmit the real part of the modulated symbol, while a second antenna transmits the imaginary part of the modulated symbol [17]. ICI is eliminated, since the data being transmitted is orthogonal and the modulation of the data is performed both on the real and imaginary parts of the carrier [17,18]. For example, in [19], antenna selection for QSM has been considered; however, the authors did not consider the application of a multicarrier QSM.

Motivated by the above, our contributions are as follows: i) we propose the design of an enhanced multicarrier modulation system, which improves the spectral efficiency/error performance of SM-OFDM in the form of QSM-OFDM. This is achieved by integrating the OFDM technology [20, 21], with QSM. QSM-OFDM eliminates ICI and inter-symbol interference (ISI), which are well-known limitations of MIMO. ii) The expressions for the computational complexities in terms of the number of real operations performed, are formulated for the proposed scheme and competing schemes. iii) Employing Monte Carlo simulations, numerical results to demonstrate the effectiveness of the proposed scheme are presented.

The remaining parts of this paper are organized as follows: Section 2 addresses the design of the QSM-OFDM system model. Section 3 analyzes the computational complexities associated with the different schemes under comparison, while the simulation results as well as related discussions are presented in Section 4. Finally, Section 5 provides necessary conclusions and recommendations.

Notation: The following notations are employed throughout this paper; bold and capital letters represent matrices, while bold small letters denote column vectors of matrices. Letters with subscript or superscript, such as  $(\cdot)_{\mathbb{R}}$  and  $(\cdot)_{\mathbb{I}}$  represents vectors or variables for real and imaginary parts, respectively. Other notations include  $(\cdot)^T$ ,  $(\cdot)^H$ ,  $(\cdot)^{-1}$ ,  $(\cdot)^\dagger$ ,  $\|\cdot\|_F$ ,  $\mathfrak{R}$  and  $\mathfrak{I}$ , which represent transpose, Hermitian, inverse, time domain signal, Frobenius norm, real part of a complex variable and time convolution, respectively. Throughout this paper,  $N_T$ ,  $N_R$  and  $M$  shall represent the

number of transmit antennas, the number of receive antennas and the MQAM modulation order, respectively.  $i = \sqrt{-1}$  represents a complex number.

## II. QSM-OFDM

### A. The QSM-OFDM Transmitter

A generalized block diagram for the system model of the proposed QSM-OFDM is shown in Figure 1. The QSM modulator in Figure 1, is like the QSM modulator in [17].

In QSM-OFDM, the input bit stream  $\mathbf{d}$  having  $N_{FFT} \log_2 MN_T^2$  bits, entering the QSM-OFDM modulator is rearranged into a  $q \times N_{FFT}$  binary matrix  $\mathbf{C}(k)$ , which is represented as:

$$\mathbf{C}(k) = \begin{bmatrix} C_{1,1} & C_{1,2} & \cdots & C_{1,q} \\ C_{2,1} & C_{2,2} & \cdots & C_{2,q} \\ \vdots & \vdots & \ddots & \vdots \\ C_{N_{FFT},1} & C_{N_{FFT},2} & \cdots & C_{N_{FFT},q} \end{bmatrix}^T \quad (1)$$

where  $N_{FFT}$  is the total number of OFDM subcarriers, which is determined by the size of the fast Fourier transform (FFT) employed,  $q$  is the total number of bits per subcarrier for a given OFDM symbol of the size  $\log_2 MN_T^2$ . The bit splitter of the QSM modulator splits each row (subcarrier) of the  $q$  bits into three different subgroups as shown in Table 1, using a  $4 \times 4$  transceiver system with 4QAM for illustration. Firstly,  $\log_2 M$  bits are used to select an MQAM symbol for the  $p$ -th subcarrier,  $x_p^m$ ,  $m \in [1: M]$  and  $p \in [1: N_{FFT}]$ .

Table 1  
Grouping of input bits for the proposed QSM-OFDM

$p$	$\mathbf{d}$ bits	Symbol bits	Real bits	Imaginary bits
1	111111	11	11	11
2	000001	00	00	01
3	101100	10	11	00
$\vdots$	$\vdots$	$\vdots$	$\vdots$	$\vdots$
$N_{FFT}$	100111	10	01	11

Another  $\log_2 N_T$  bits are employed to select the  $\ell_{\mathbb{R}_p}$ -th antenna for transmitting the real part of the complex variable  $x_p^m$  of the  $p$ -th subcarrier, and the third subgroup of  $\log_2 N_T$  bits are employed to select the  $\ell_{\mathbb{I}_p}$ -th antenna for transmitting the imaginary part of the complex variable  $x_p^m$  of the  $p$ -th subcarrier, where  $\ell_{\mathbb{R}_p}, \ell_{\mathbb{I}_p} \in [1: N_T]$ . The bit processing of Table 1 is presented in Table 2.

Table 2  
Outputs from the QSM modulator

$p$	$x_p^m$	$x_p^{m,\mathbb{R}}$	$x_p^{m,\mathbb{I}}$	$\ell_{\mathbb{R}_p}$	$\ell_{\mathbb{I}_p}$	$\mathbf{x}_{QSM-OFDM}^p$
1	$+1+i$	+1	+i	4	4	$[0 \ 0 \ 0 \ +1+i]^T$
2	$-1-i$	-1	-i	1	2	$[-1 \ -i \ 0 \ 0]^T$
3	$+1-i$	+1	-i	4	1	$[-i \ 0 \ 0 \ +1]^T$
$\vdots$	$\vdots$	$\vdots$	$\vdots$	$\vdots$	$\vdots$	$\vdots$
$N_{FFT}$	$+1-i$	+1	-i	2	4	$[0 \ +1 \ 0 \ -i]^T$

The symbol  $x_p^m$  is further decomposed into its real  $x_p^{m,\mathbb{R}}$  and imaginary  $x_p^{m,\mathbb{I}}$  components, such that:

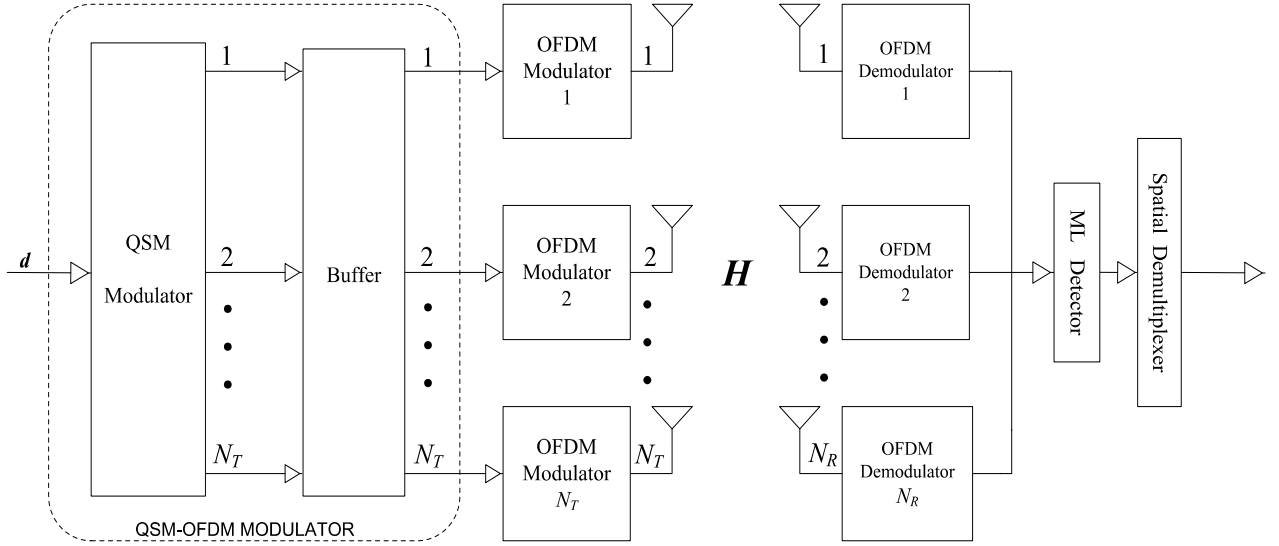


Figure 1: System model of the proposed QSM-OFDM

$$\mathbf{x}_p^m = \mathbf{x}_p^{m,\mathfrak{R}} + i\mathbf{x}_p^{m,\mathfrak{I}} \quad (2)$$

These components are then mapped to form the vectors for the  $N_T$  OFDM symbols of the  $p$ -th subcarrier, such that:

$$\mathbf{x}_{QSM-OFDM}^p = \mathbf{x}_{\ell_{\mathfrak{R}p}}^{m,\mathfrak{R}} + i\mathbf{x}_{\ell_{\mathfrak{I}p}}^{m,\mathfrak{I}} \quad (3)$$

where  $\mathbf{x}_{\ell_{\mathfrak{R}p}}^{m,\mathfrak{R}}$  and  $\mathbf{x}_{\ell_{\mathfrak{I}p}}^{m,\mathfrak{I}}$  are  $N_T \times 1$  vectors with  $x_p^{m,\mathfrak{R}}$  and  $i x_p^{m,\mathfrak{I}}$  as the non-zero entry placed at the  $\ell_{\mathfrak{R}p}$ -th and  $\ell_{\mathfrak{I}p}$ -th positions, respectively, for the  $p$ -th subcarrier,  $p \in [1: N_{FFT}]$ . The outputs from the QSM modulator  $\mathbf{x}_{QSM-OFDM}^p$ , when  $\ell_{\mathfrak{R}p} \neq \ell_{\mathfrak{I}p}$  is of the form represented as:

$$\mathbf{x}_{QSM-OFDM}^p = \begin{bmatrix} 0 \cdots 0 & \underbrace{x_p^{m,\mathfrak{R}}}_{\ell_{\mathfrak{R}p}\text{-th position}} & 0 \cdots 0 & \underbrace{i x_p^{m,\mathfrak{I}}}_{\ell_{\mathfrak{I}p}\text{-th position}} & 0 \cdots 0 \end{bmatrix}^T \quad (4)$$

and when  $\ell_{\mathfrak{R}p} = \ell_{\mathfrak{I}p}$ ,  $\mathbf{x}_{QSM-OFDM}^p$  takes the form:

$$\mathbf{x}_{QSM-OFDM}^p = \begin{bmatrix} 0 \cdots 0 & \underbrace{x_p^{m,\mathfrak{R}} + i x_p^{m,\mathfrak{I}}}_{\ell_{\mathfrak{R}p}\text{-th} = \ell_{\mathfrak{I}p}\text{-th position}} & 0 \cdots 0 \end{bmatrix}^T \quad (5)$$

The outputs of the QSM modulator  $\mathbf{x}_{QSM-OFDM}^p$ , forms the matrix  $\mathbf{J}$ , such that  $\mathbf{J}$  is an  $N_T \times N_{FFT}$  frequency domain matrix represented as:

$$\mathbf{J} = \begin{bmatrix} j_1[1] & j_1[2] & \cdots & j_1[N_{FFT}] \\ j_2[1] & j_2[2] & \cdots & j_2[N_{FFT}] \\ \vdots & \vdots & \ddots & \vdots \\ j_{N_T}[1] & j_{N_T}[2] & \cdots & j_{N_T}[N_{FFT}] \end{bmatrix} \quad (6)$$

where each column  $p$ , of  $\mathbf{J}$  represents the data to be transmitted on the  $p$ -th subcarrier, while the row  $\ell$ , of  $\mathbf{J}$  are the OFDM symbols to be transmitted by the  $\ell$ -th antenna,  $\ell \in [1: N_T]$ . For example,  $j_\ell[p]$  is the data on the  $p$ -th subcarrier

of the  $\ell$ -th OFDM symbol and will be transmitted employing the  $\ell$ -th transmit antenna.

The OFDM modulator processes the signal to obtain the complex baseband time domain signals by performing an inverse FFT (IFFT), which may be expressed as:

$$\mathbf{x}_t^\dagger = \frac{1}{\sqrt{N_{FFT}}} \sum_{p=0}^{N_{FFT}-1} J_\ell(p) e^{\frac{i2\pi t p}{N_{FFT}}} \quad (7)$$

where  $\mathbf{x}_t^\dagger$  is the time domain signal obtained at the  $t$ -th time interval of the  $\ell$ -th transmit antenna. This process is followed by the addition of a cyclic prefix (CP) to eliminate ISI before the onward simultaneous transmission by  $N_T$  transmit antennas via the MIMO channel  $\mathbf{H}$ .

### B. The QSM-OFDM Receiver

At the receiver, the transmitted data encounters the additive white Gaussian noise (AWGN). The received time domain signal vector  $\mathbf{Y}^\dagger(t)$ , at any time  $t$ , may be represented as:

$$\mathbf{Y}^\dagger(t) = \mathbf{H}^\dagger(t, \tau) \otimes \mathbf{X}^\dagger(t) + \mathbf{W}^\dagger(t) \quad (8)$$

where  $\mathbf{H}^\dagger(t, \tau)$  is the time domain multipath channel matrix with a delay spread  $\tau$  arriving at time  $t$ . The frequency domain representation of  $\mathbf{H}^\dagger(t, \tau)$  at any time  $t$ , for the  $p$ -th subcarrier may be defined as:

$$\mathbf{H}_p = \begin{bmatrix} h_{1,1} & h_{1,2} & \cdots & h_{1,N_T} \\ h_{2,1} & h_{2,2} & \cdots & h_{2,N_T} \\ \vdots & \vdots & \ddots & \vdots \\ h_{N_R,1} & h_{N_R,2} & \cdots & h_{N_R,N_T} \end{bmatrix} \quad (9)$$

and  $\mathbf{W}^\dagger(t)$  is the AWGN matrix at the receiver, whose entries are independent and identically distributed (i.i.d.) random variables with distribution  $CN(0, \sigma_W^2)$ . The received time domain signal  $\mathbf{Y}^\dagger(t)$  is demodulated by employing a bank of  $N_R$  OFDM demodulators, while the OFDM demodulator removes the CP and performs the FFT operation. The

frequency domain output for a single subcarrier may be represented as:

$$\mathbf{y}_p = \sqrt{\rho} \left( \mathbf{h}_{\ell_{\Re}}^p x_{\Re}^p + i \mathbf{h}_{\ell_{\Im}}^p x_{\Im}^p \right) + \mathbf{w}_p \quad (10)$$

where  $\mathbf{y}_p$ ,  $p \in [1: N_{FFT}]$  is the frequency domain vector of the received signal for the  $p$ -th subcarrier of the OFDM symbol,  $\mathbf{h}_{\ell_{\Re}}^p = [h_{1,\ell_{\Re}}^p \ h_{2,\ell_{\Re}}^p \ \dots \ h_{N_R,\ell_{\Re}}^p]^T$  represents the  $N_R \times 1$   $\ell_{\Re}$ -th column vector of the frequency response channel matrix  $\mathbf{H}_p$  for the real variables of the  $p$ -th subcarrier of the OFDM symbol.  $\mathbf{h}_{\ell_{\Im}}^p = [h_{1,\ell_{\Im}}^p \ h_{2,\ell_{\Im}}^p \ \dots \ h_{N_R,\ell_{\Im}}^p]^T$  is the  $N_R \times 1$   $\ell_{\Im}$ -th column vector of the frequency response of the channel matrix  $\mathbf{H}_p$ , for the imaginary variables of the  $p$ -th subcarrier of the OFDM symbol.  $x_{\Re}^p$  and  $x_{\Im}^p$  represent the real and imaginary complex variables, respectively, that are transmitted, and  $\mathbf{w}_p$  is the AWGN for the  $p$ -th subcarrier of the OFDM symbol, whose entries are i.i.d. with a distribution of  $CN(0, \sigma^2)$ .  $\rho = \frac{E_s}{N_T}$ , and  $E_s$  is the energy of the transmitted symbol. The receiver implements a joint ML detection scheme over all possible symbols with the assumption of perfect knowledge of the channel. The equation for the joint ML detector as it applies to QSM-OFDM adopted from [17] may be represented as:

$$\begin{aligned} [\hat{\ell}_{\Re}, \hat{\ell}_{\Im}, \hat{u}_{\Re}, \hat{u}_{\Im}] = \operatorname{argmin}_{\ell_{\Re}, \ell_{\Im}, u_{\Re}, u_{\Im}} \left\| \mathbf{y}_p \right. \\ \left. - \sqrt{\rho} \left( \mathbf{h}_{\ell_{\Re}}^p x_{\Re}^p + i \mathbf{h}_{\ell_{\Im}}^p x_{\Im}^p \right) \right\|_F^2 \end{aligned} \quad (11)$$

where  $\hat{\ell}_{\Re}$  and  $\hat{\ell}_{\Im}$  are the detected antenna indices for the antennas transmitting the real and imaginary symbols for the  $p$ -th subcarrier, respectively, for  $\ell_{\Re}, \ell_{\Im} \in [1: N_T]$ , and  $\hat{u}_{\Re}$  and  $\hat{u}_{\Im}$  are the detected estimates for the real and the imaginary symbols  $u_{\Re}$  and  $u_{\Im}$  for the  $p$ -th subcarrier,  $\hat{u}_{\Re}, \hat{u}_{\Im} \in [1: M]$ .

A further simplification of (11) gives:

$$\begin{aligned} [\hat{\ell}_{\Re}, \hat{\ell}_{\Im}, \hat{u}_{\Re}, \hat{u}_{\Im}] = \operatorname{argmin}_{\ell_{\Re}, \ell_{\Im}, u_{\Re}, u_{\Im}} \left\| \mathbf{g} \right\|_F^2 \\ - 2\Re \left( (\mathbf{y}_p)^H \mathbf{g} \right) \end{aligned} \quad (12)$$

where  $\mathbf{g} = \sqrt{\rho} \left( \mathbf{h}_{\ell_{\Re}}^p x_{\Re}^p + i \mathbf{h}_{\ell_{\Im}}^p x_{\Im}^p \right)$ .

The estimates  $\hat{\ell}_{\Re}$ ,  $\hat{\ell}_{\Im}$ ,  $\hat{u}_{\Re}$  and  $\hat{u}_{\Im}$ , are spatially demultiplexed to obtain the detected bits at the output.

### III. RECEIVER COMPUTATIONAL COMPLEXITY ANALYSIS

This section presents a comparison of the receiver computational complexities for the different systems being compared with the proposed QSM-OFDM, viz; Alamouti-OFDM, VBLAST-OFDM, SM-OFDM and the single-input multiple-output OFDM system, which employs maximal-ratio combining detector (MRC-OFDM). In this paper, the computational complexities are resolved to the number of real multiplications and additions being carried out at the receiver [22]. It should be noted that where possible, the arithmetic path that gives the lower computational complexity in achieving a given detection at the receiver is assumed, and

the total complexity is the sum of the real multiplications and real additions for each subcarrier. As a background for the calculation of computational complexities in terms of real operations performed during processing, a complex multiplication (CM) is achieved by performing four real multiplications ( $4m$ ) and two real additions ( $2a$ ), which makes a total of 6 real operations, while a complex addition (CA) is obtained by performing  $2a$ , as explained in [22].

#### A. QSM-OFDM

The total computational complexity for the proposed QSM-OFDM for a single subcarrier is given as:

$$\delta_{\text{QSM-OFDM}} = 25MN_T^2N_R + 3MN_T^2 - 1 \quad (13)$$

The  $\|\mathbf{g}\|_F^2$  in (12) is obtained by  $10N_Rm$  and  $8N_Ra$ .  $(\mathbf{y}_p)^H \mathbf{g}$  is obtained by  $4N_Rm + (3N_R - 1)a$ , since  $\mathbf{g}$  is stored and there is no need for recalculation. Additional  $m + a$  is used to obtain  $\|\mathbf{g}\|_F^2 - 2\Re \left( (\mathbf{y}_p)^H \mathbf{g} \right)$ . However, there are  $MN_T^2$  iterations of  $\|\mathbf{g}\|_F^2 - 2\Re \left( (\mathbf{y}_p)^H \mathbf{g} \right)$ , after which the  $MN_T^2$  outputs are compared using  $(MN_T^2 - 1)a$  to obtain a minimum value, thus, making the computational complexity in terms of real operations  $MN_T^2(14N_R + 1)m + (11MN_T^2N_R + 2MN_T^2 - 1)a$ .

#### B. MRC-OFDM

The product  $\mathbf{H}^H \mathbf{Y}$  yields  $N_T N_R$  CM and  $N_T N_R - N_T$  CA, which can be achieved by  $4N_T N_R m + 2N_T(2N_R - 1)a$ . The product  $\mathbf{H}^H \mathbf{H}$  has  $N_T^2 N_R$  CM and  $N_T^2 N_R - N_T^2$  CA obtained by performing  $4N_T^2 N_R m + (4N_T^2 N_R - 2N_T^2)a$ . The division  $\frac{\mathbf{H}^H \mathbf{Y}}{\mathbf{H}^H \mathbf{H}}$  is performed by using  $2m$ . The computational complexity needed to obtain an estimate of the transmitted symbol is ignored because a one-to-one mapping is performed [23]. Thus, MRC-OFDM has  $(4N_T^2 N_R + 4N_T N_R + 2)m + (4N_T^2 N_R - 2N_T^2 + 4N_T N_R - 2N_T)a$ , giving a total complexity for MRC-OFDM as:

$$\delta_{\text{MRC-OFDM}} = 8N_T^2 N_R - 2N_T^2 + 8N_T N_R - 2N_T + 2 \quad (14)$$

#### C. Alamouti-OFDM

The computational complexity for  $\|\mathbf{g}\|_F^2 - 2\Re \left( (\mathbf{y}_p)^H \mathbf{g} \right)$  imposed by the Alamouti ML detector, is similar to subsection III.A and requires  $25N_R + 1$  operations. The number of iterations the detector performs is  $M^2$ , hence, to determine the minimum, the ML detector requires  $(M^2 - 1)a$  operations. Since the detection performed is for two MQAM symbols, thus, the total complexity for a single subcarrier is obtained by dividing the total number of real operations by 2, which gives:

$$\delta_{\text{Alamouti-OFDM}} = \frac{1}{2} (25N_R M^2 - M^2 - 25N_R - 1) \quad (15)$$

#### D. VBLAST-OFDM

Depending on the VBLAST detection algorithm being used, the computational complexities can vary in different ways. Using the MMSE-OSIC described in [3], the CM imposed is given as  $N_T^3 + 2N_T^2 N_R + N_R$ . This value is

obtained by the multiplications of the channel matrix and an inverse matrix, hence resulting in  $(4N_T^3 + 8N_T N_R + 4N_R)m + (2N_T^3 + 4N_T N_R + 2N_R)a$ . A minimum of  $N_T^3 + 2N_T^2 N_R - N_T^2 - N_T N_R + N_R - 1$  CA were made in actualizing this, resulting in  $2(N_T^3 + 2N_T^2 N_R - N_T^2 - N_T N_R + N_R - 1)a$ . The total number of operations in terms of  $m$  and  $a$  employed to determine the layer having the minimum estimation error of  $G_{MMSE}$  in ([3], (11)) i.e., the layer having the minimum Euclidean norm is given as  $2N_T N_R m + (N_T N_R + N_T - 1)a$ . The computational complexity of the quantization slicing function  $\Psi(G_{MMSE} \times \mathbf{y}_p)$ , which is used to estimate the transmitted symbol is ignored because, a one-to-one mapping is performed [23]. The total number of real operations to be carried out by a receiver in detecting the transmitted symbol by a single transmit antenna is given as:

$$10N_T^3 + 4N_T^2 N_R - 2N_T^2 + 13N_T N_R + 8N_R + N_T - 3 \quad (16)$$

Since the technique used for the VBLAST-OFDM recursively decreases in the number of transmit antennas  $N_T$  due to the elimination of detected symbols, the overall number of real operations can be written as:

$$\delta_{\text{VBLAST-OFDM}} = \sum_{\ell=1}^{N_T} (10N_{T,\ell}^3 + 4N_{T,\ell}^2 N_R - 2N_{T,\ell}^2 + 13N_{T,\ell} N_R + 8N_R + N_{T,\ell} - 3) \quad (17)$$

where  $N_{T,\ell}$  is the number of transmit antennas for the  $\ell$ -th,  $\ell \in [1: N_T]$  iteration.

#### E. SM-OFDM

The SM-OFDM ML detection process requires  $(4N_R + 2N_T N_R)m + (5N_R + N_T N_R - 1)a$ , while a total of  $MN_T$  iterations and  $(MN_T - 1)a$  operations are employed to obtain the minimum from the Frobenius norms. The total number of real operations can then be given as:

$$\delta_{\text{SM-OFDM}} = MN_T(3N_T N_R + 9N_R - 1) \quad (18)$$

Table 3 summarizes the computational complexities per subcarrier for the different OFDM schemes and are pictorially represented by the bar chart in Figure 2.

Table 3  
Grouping of input bits for the proposed QSM-OFDM

SYSTEM	4 bits/s/Hz	6 bits/s/Hz	8 bits/s/Hz
VBLAST-OFDM	550	550	4,516
SM-OFDM	944	5,312	21,248
QSM-OFDM	1,647	6,591	26,367
Alamouti-OFDM	10,496	167,936	2,686,976

The axis on the right (secondary axis) indicates values for the computational complexity of Alamouti-OFDM, because of the high computational complexity, while the axis on the left (primary axis) is for the other schemes, such as VBLAST-

OFDM, SM-OFDM and QSM-OFDM being compared in our work. The ALAMOUTI-OFDM scheme has a very high computational complexity when compared with other schemes in this paper.

There is a 24% increase in the computational complexity (in terms of real operations) of the proposed QSM-OFDM scheme over the SM-OFDM, when the spectral efficiency for each subcarrier of the OFDM symbol is high (6 bits/s/Hz and 8 bits/s/Hz), such as seen in Table 3 and Figure 2.

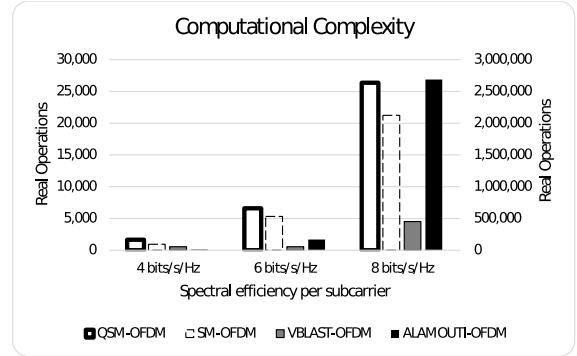


Figure 2: Bar chart showing the computational complexities of QSM-OFDM and competing schemes

However, there is a 74% increase in the computational complexity of QSM-OFDM over SM-OFDM, when the spectral efficiency is 4 bits/s/Hz. The VBLAST-OFDM is seen to have the lowest computational complexity in all the schemes compared. However, because the RF chains of VBLAST increases with the number of transmit antenna, it is more prone to ICI. Furthermore, the complexity involved in the design is higher due to inter-antenna synchronization (IAS). Nevertheless, it has been included for comparison purposes.

#### IV. SIMULATION RESULTS AND DISCUSSION

In this section, we quantify the bit error rate (BER) performance demonstrated by the proposed QSM-OFDM scheme employing Monte Carlo simulations. Simulations were performed for 4, 6 and 8 bits/s/Hz as shown in Figure 3, 4 and 5, respectively. Parameters employed for the simulations are given in Table 4 [1], while Table 5 compares the BER performance of QSM-OFDM with other schemes.

Table 4  
Parameters for simulation [1]

PARAMETERS	VALUE
CP	32
Carrier frequency	2 GHz
Number of subcarriers	256
Antenna Configurations	2 × 4 and 4 × 4
Channel Property	ITU EPA model
Modulation Scheme	MQAM

The following assumptions were made for the simulations; multipath channels are statistically independent for the different pathways, time and frequency synchronization is perfect and the total signal power is the same for all transmission, while AWGN is assumed in all cases. In all schemes used for comparison in this paper, the ML detector

Table 5  
Comparison of BER performances of QSM-OFDM over competing schemes

SCHEME	4 bits/s/Hz		6 bits/s/Hz		8 bits/s/Hz	
	CONFIGURATION	GAIN (dB)	CONFIGURATION	GAIN (dB)	CONFIGURATION	GAIN (dB)
MIMO-OFDM	2 × 4 16QAM	2	4 × 4 64QAM	5	4 × 4 256QAM	> 15
SM-OFDM	2 × 4 8QAM	4	4 × 4 16QAM	4	4 × 4 64QAM	≈ 5
Alamouti-OFDM	2 × 4 16QAM	7	2 × 4 64QAM	12	4 × 4 256QAM	> 20
MRC-OFDM	1 × 4 16QAM	2	1 × 4 64QAM	5	1 × 4 256QAM	> 15
VBLAST-OFDM	2 × 4 4QAM	-2	2 × 4 8QAM	1	4 × 4 4QAM	≈ 2

is employed. However, due to the impracticality of employing the ML detector in the VBLAST-OFDM system, because of the computational complexity, which requires  $MN_T$  iterations per subcarrier, the optimal minimum mean square error (MMSE) detection, which is combined with the ordered successive interference cancellation (OSIC) as used in [3], is employed in VBLAST-OFDM simulation of this paper.

Considering Figure 3, there is a major improvement of the proposed QSM-OFDM greater than 3 dB in SNR over the SM-OFDM at a BER of  $10^{-5}$ . Also, a significant improvement of QSM-OFDM over the Alamouti-OFDM scheme greater than 7 dB in SNR at a BER of  $10^{-5}$ , while the QSM-OFDM outperforms the MIMO-OFDM and MRC-OFDM by approximately 2 dB in SNR at the same BER. VBLAST-OFDM shows a slightly better error performance of  $\approx 1$  dB in SNR over QSM-OFDM. However, VBLAST-OFDM suffers from high ICI as all antennas are made to transmit different symbols. Also, the need for IAS is a major disadvantage for VBLAST-OFDM as the number of RF chains increase with the number of transmit antennas.

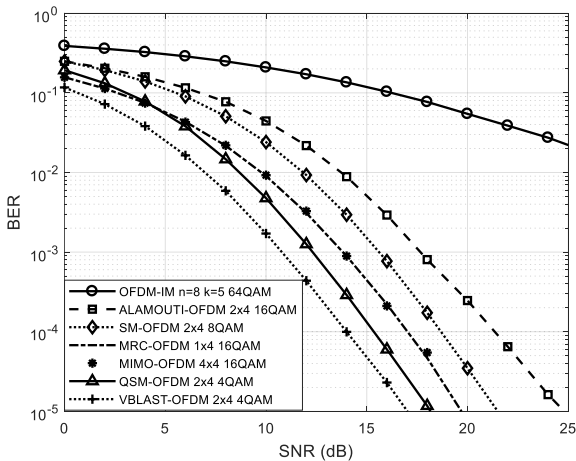


Figure 3. BER versus SNR for 4 bits/s/Hz for QSM-OFDM and other schemes.

In Figure 4, the proposed QSM-OFDM outperforms the SM-OFDM, MIMO-OFDM and MRC-OFDM with SNR gain  $\geq 5$  dB at a BER of  $10^{-5}$ . This is achieved when a  $4 \times 4$  antenna configuration is used with 4QAM for QSM-OFDM, to obtain a 6 bits/s/Hz transmission per subcarrier. However, a 2 dB gain in SNR is observed, when a  $2 \times 4$  antenna configuration is used with 16QAM at a BER of  $10^{-5}$ . The Alamouti-OFDM require additional power of  $\approx 10$  dB to attain a BER of  $10^{-3}$  as QSM-OFDM. The VBLAST-OFDM has a slightly better error performance of approximately 1.5 dB in SNR over QSM-OFDM at a BER of  $10^{-5}$ , when the same number of transmit antennas are employed. However,

when the number of transmit antennas for QSM-OFDM is increased for the same spectral efficiency per subcarrier, the QSM-OFDM is seen to outperform VBLAST-OFDM at higher SNR. Furthermore, due to the limitations of VBLAST-OFDM mentioned earlier, the QSM-OFDM in this regard, remains as a better candidate for modern communication systems.

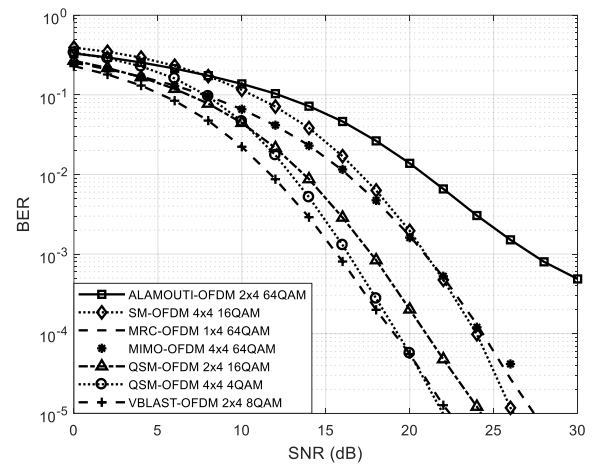


Figure 4. BER versus SNR for 6 bits/s/Hz for QSM-OFDM and other schemes.

Considering Figure 5, which is the 8 bits/s/Hz transmission for a given subcarrier, the proposed QSM-OFDM outperforms the SM-OFDM scheme by approximately 5 dB when the BER is  $10^{-5}$ . Higher SNR gain is recorded when QSM-OFDM is compared with other schemes.

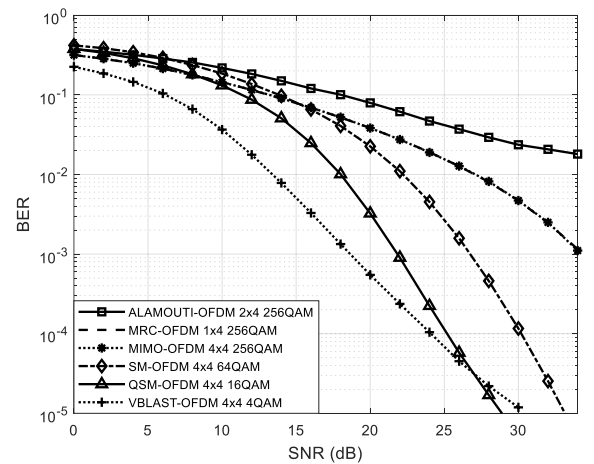


Figure 5. BER versus SNR for 8 bits/s/Hz for QSM-OFDM and other schemes

Typically, schemes like Alamouti-OFDM and MIMO-OFDM will need a very high SNR, greater than 35 dB to attain a BER of  $10^{-5}$ . Also, the QSM-OFDM is seen to

outperform VBLAST-OFDM at higher SNR. A summary of the BER performance of the proposed QSM-OFDM system being compared with other OFDM systems is presented in Table 5.

The error performance of QSM-OFDM over SM-OFDM is  $\approx 4$  dB gain in SNR, when 4 bits/s/Hz is used for each subcarrier of the OFDM symbol. The gain in error performance is maintained with a narrow increase when the 6 bits/s/Hz and 8 bits/s/Hz are used, respectively. The error performance of QSM-OFDM over Alamouti-OFDM is highest. It is seen to increase, when the spectral efficiency per subcarrier being used for the QSM-OFDM system is increased. When QSM-OFDM is compared with MIMO-OFDM and MRC-OFDM, its error performance is minimal ( $\approx 2$  dB) when a 4 bits/s/Hz is used for each subcarrier of the OFDM symbol but increases to 5 dB and 15 dB when 6 bits/s/Hz and 8 bits/s/Hz are used, respectively.

## V. CONCLUSION

This paper has analyzed the potency in exploiting the spatial domain as a means of increasing the spectral efficiency of the system and benefiting from the gains of OFDM in eliminating ISI and co-channel interference. The results showed that the proposed QSM-OFDM has a better error performance than the SM-OFDM system without additional cost of hardware. Also, SM-OFDM will need a minimum of 4 dB signal power to attain the same BER of QSM-OFDM, if the spectral efficiency is made constant. The proposed QSM-OFDM scheme displayed superior error performance over MRC-OFDM, MIMO-OFDM, and Alamouti-OFDM. From the results, QSM-OFDM also demonstrates a better error performance than VBLAST-OFDM at high SNR. Since the number of RF chains for VBLAST-OFDM increases with the number of transmit antennas it becomes more susceptible to ICI and IAS than QSM-OFDM. Hence, the proposed QSM-OFDM scheme becomes the preferred candidate for modern day communication. Since recent research has focused on energy and spectral efficient devices, QSM-OFDM becomes a more promising model for future wireless communication as its design is implementable for the OFDM system.

## REFERENCES

- [1] S. U. Hwang, S. Jeon, S. Lee, and J. Seo, "Soft-output ML detector for spatial modulation OFDM systems," *IEICE Electronics Express*, vol. 6, no. 19, pp. 1426-1431, Oct. 2009.
- [2] P. Yang, M. D. Renzo, Y. Xiao, S. Li, and L. Hanzo, "Design Guidelines for Spatial Modulation," *IEEE Communications Surveys & Tutorials*, vol. 17, no. 1, pp. 6-26, Firstquarter 2015.
- [3] R. Bohnke, D. Wubben, V. Kuhn, and K. D. Kammeyer, "Reduced complexity MMSE detection for BLAST architectures," in *Proc. IEEE Global Telecommunications Conference (GLOBECOM 2003)*, pp. 2258-2262 vol.4, Dec. 2003.
- [4] V. Tarokh, N. Seshadri, and A. R. Calderbank, "Space-time codes for high data rate wireless communication: performance criterion and code construction," *IEEE Transactions on Information Theory*, vol. 44, no. 2, pp. 744-765, Mar. 1998.
- [5] R. Y. Mesleh, H. Haas, S. Sinanovic, C. W. Ahn, and S. Yun, "Spatial Modulation," *IEEE Transactions on Vehicular Technology*, vol. 57, no. 4, pp. 2228-2241, Jul. 2008.
- [6] N. Pillay and X. Hongjun, "Low-complexity transmit antenna selection schemes for spatial modulation," *IET Communications*, vol. 9, no. 2, pp. 239-248, Jan. 2015.
- [7] J. Wang, S. Jia, and J. Song, "Generalised Spatial Modulation System with Multiple Active Transmit Antennas and Low Complexity Detection Scheme," *IEEE Transactions on Wireless Communications*, vol. 11, no. 4, pp. 1605-1615, Mar. 2012..
- [8] J. Jeganathan, A. Ghrayeb, L. Szczecinski, and A. Ceron, "Space shift keying modulation for MIMO channels," *IEEE Transactions on Wireless Communications*, vol. 8, no. 7, pp. 3692-3703, Jul. 2009.
- [9] J. Jeganathan, A. Ghrayeb, and L. Szczecinski, "Generalized space shift keying modulation for MIMO channels," in *Proc. IEEE 19th International Symposium on Personal, Indoor and Mobile Radio Communications (PIMRC 2008)*, pp. 1-5, Sep. 2008.
- [10] K. Kadathal, H. Xu and N. Pillay, "Generalised differential scheme for spatial modulation systems," *IET Communications*, vol. 11, no. 13, pp. 2020-2026, 2017.
- [11] M. D. Renzo, H. Haas, A. Ghrayeb, S. Sugiura, and L. Hanzo, "Spatial Modulation for Generalized MIMO: Challenges, Opportunities, and Implementation," *Proceedings of the IEEE*, vol. 102, no. 1, pp. 56-103, Jan. 2014.
- [12] H.-W. Liang, R. Y. Chang, W.-H. Chung, H. Zhang, and S.-Y. Kuo, "Bi-space shift keying modulation for MIMO systems," *IEEE Communications Letters*, vol. 16, no. 8, pp. 1161-1164, Jun. 2012.
- [13] K. Govindasamy, H. Xu, and N. Pillay, "Space-time block coded spatial modulation with labeling diversity," *International Journal of Communication Systems*, vol. 31, no. 1, 2018.
- [14] S. Ganesan, R. Mesleh, H. Ho, C. W. Ahn, and S. Yun, "On the Performance of Spatial Modulation OFDM," in *Proc. Fortieth Asilomar Conference on Signals, Systems and Computers*, pp. 1825-1829, Oct. 2006.
- [15] Y. S. Cho, J. Kim, W. Y. Yang, and C. G. Kang, *MIMO-OFDM wireless communications with MATLAB*: John Wiley & Sons, 2010.
- [16] F. Yu, X. Lei, L. Peng, Y. Xiao, P. Wei, and X. Wen, "Performance Analysis of Spatial Modulation OFDM System with N-Continuous Precoder," in *Proc. IEEE 83rd Vehicular Technology Conference (VTC Spring)*, pp. 1-5, May 2016.
- [17] R. Mesleh, S. S. Ikki, and H. M. Aggoune, "Quadrature Spatial Modulation," *IEEE Transactions on Vehicular Technology*, vol. 64, no. 6, pp. 2738-2742, Jun. 2015.
- [18] L. Xiao, P. Yang, S. Fan, S. Li, L. Song, and Y. Xiao, "Low-Complexity Signal Detection for Large-Scale Quadrature Spatial Modulation Systems," *IEEE Communications Letters*, vol. 20, no. 11, pp. 2173-2176, Aug. 2016.
- [19] S. Naidu, and N. Pillay, and H. Xu, "Transmit Antenna Selection Schemes for Quadrature Spatial Modulation," *Wireless Personal Communications*, vol. 99, no. 1, pp. 299-317, 2018.
- [20] R. W. Chang, "Synthesis of Band - Limited Orthogonal Signals for Multichannel Data Transmission," *Bell System Technical Journal*, vol. 45, no. 10, pp. 1775-1796, Dec. 1966.
- [21] B. Saltzberg, "Performance of an efficient parallel data transmission system," *IEEE Transactions on Communication Technology*, vol. 15, no. 6, pp. 805-811, Dec. 1967.
- [22] A. M. Elshokry, "Complexity and performance evaluation of detection schemes for spatial multiplexing mimo systems," Faculty of Engineering, Islamic University Gaza, 2010.
- [23] H. Xu, "Simplified maximum likelihood-based detection schemes for M-ary quadrature amplitude modulation spatial modulation," *IET Communications*, vol. 6, no. 11, pp. 1356-1363, Jul. 2012.